Proceedings of the Thirty-second (2022) International Ocean and Polar Engineering Conference **www.isope.org**
Shanghai, China, June 5–10, 2022

ISBN 978-1-880653-81-4; ISSN 1098-6189

SPH Method for Impact Load of Water Spray Generated by the Landing Gear

Xiangshan Guan[1], Ruosi Zha[1], Decheng Wan[2]*

[1]School of Ocean Engineering and Technology, Sun Yat-Sen University, Zhuhai, Guangdong, China
[2]Computational Marine Hydrodynamic Lab (CMHL), School of Naval Architecture, Ocean and Civil Engineering, Shanghai Jiao Tong University, Shanghai, China
*Corresponding author

ABSTRACT

In this paper, the impact load of water spray under the influence of air is calculated, and an efficient and accurate calculation method is proposed. Firstly, the initial patterns of tire water spray are simulated by the SPH-FEM method in LS-DYNA, then the position and velocity information of SPH particles is exported. Secondly, the SPH particles are regarded as droplets, and the droplets load is calculated by the Monte Carlo method according to the droplet impact load curve. The distribution of droplets was modified according to the relationship between time and space. Finally, the corrected impact load of water spray is obtained. The calculated values are in good agreement with the measured values obtained by the tire drop experiment, which proves the validity of the method.

KEYWORDS: SPH method, impact load, tire spray, tire drop experiment, Monte Carlo method

INTRODUCTION

Although the take-off and landing stages are short, they are the most accident-prone stages. When an aircraft passes through a wet runway, the tire water spray may enter the engine and affect the operation of the engine, and the water spray may also impact the aircraft fuselage and cause structural damage (Van Es G W H, Roelen A L C, Kruijsen E A C, 1998). To ensure the safety of aircraft, the FAA (Federal Aviation Administration) had issued regulation AC-91-6A, which establishes flight guidelines for slippery, waterlogged or contaminated runways.

Therefore, the wet runway flight test is an essential process for civil aircraft to obtain airworthiness certification, but it is expensive to conduct frequent flight tests of the whole aircraft. With the increasing computing power of the computer, the water body can be refined continuously. As a result, the calculation results of spray patterns and water distribution can be more accurate, providing a reference for flight tests or even replacing some tests in the early stage. The numerical method effectively shortens the time to obtain airworthiness certification and save test cost.

Among the effects of tire water spray, the impact of water spray on aircraft structures cannot be ignored. High-speed droplets hit the aircraft fuselage, wind speed ducts, engine blades and other critical locations, which may adversely affect aircraft safety and performance. Therefore, simulating the spray patterns and calculating the impact load is an important part of the numerical simulation of tire water spray. There are many numerical studies related to tire water spray. In 1998, ESDU proposed an engineering method to calculate the patterns of the side spray according to a large number of test results. This method calculated and described the parameters of side spray patterns, such as spray height, sputter angle, and so on, according to the basic parameters such as tire parameters, depth of water accumulation, aircraft speed, and so on. In 2013, the CR-SPRAY method using the Monte Carlo method was proposed by Gooden J H M. According to the initial patterns of tire spray obtained by the ESDU method, the particle trajectory algorithm was used to calculate the complete splashing trajectory. Liu et al. used the SPH method to simulate the tire spray and simulated the splashing trajectory in the discrete phase model method. They obtained the water spray patterns of the nose gear, which were in good agreement with the test results of ARJ21(Zhao K, Liu P Q, Qu Q L, 2018). In the meantime, Xu et al. studied the water spray of elastic large deformation tires by the SPH method and studied the tire hydroplaning phenomenon (Xianpeng ZHANG, Fei XU, Xuanqi REN, 2019). However, these studies mainly focus on the spray patterns (Guan Xiangshan, Xu Fei, Hu Muqiu, 2021), and relatively few calculations are performed for the impact load of tire water spray. Because the computational domain of tire water spray is huge, if the complete process of tire water spray is simulated throughout and the impact load of spray is calculated, the calculation time will be very long.

Although it is difficult to use the SPH method to simulate the complete process of tire spray, the SPH method can be used to obtain the initial patterns of the tire spray accurately. SPH method is a meshless method. The meshless method obtains accurate and stable numerical solutions using a series of arbitrarily distributed nodes (or particles) to solve integral equations or partial differential equations (PDEs) with different boundary conditions. These nodes (or particles) do not require mesh connections, which can easily solve the large deformation, moving interface and free surface problems encountered during numerical simulation. The SPH method could avoid the precision damage caused by mesh distortion when extremely large deformation appears, and it would be flexible by using the SPH method in dealing with the large deformation and breaking of liquid. The SPH method has been widely used in many practical problems (Khayyer A, You Y, Gotoh H, 2021), such as incompressible flow, explosion shock, high-speed compressible flow, underwater explosion, free surface flow, and so on (Luo Min, Khayyer A).

In this paper, a more efficient calculation method pf tire spray load is proposed. First, a small-size tire drop experiment is conducted to obtain the impact load of tire spray on the fixed sensor. At the same time, the SPH-FEM method is used in LS-DYNA to build a tire spray model of the same size, simulate the tire spray pattern and obtain the distribution of splashing particles. Then the splashing particles are regarded as droplets, and their trajectory in the airflow field is calculated. Finally, the impact load of the droplets on the sensor is calculated and compared with the experimental results.

TIRE DROP EXPERIMENT

Phenomenon of tire spray

The phenomenon of tire spray belongs to a typical shallow water impact problem. The tire squeezes the water film during the wading process, and the water film is deformed under pressure, which leads to the water film breaking and liquid droplets splashing. The tire spray is formed after a series of complex processes such as droplet collision and convergence. The tire spray is mainly divided into three parts: bow wave, side spray and tail wave. The bow wave is splashed from the front of the tire, and the side spray is splashed from the sides of the tire. The viscosity force makes a small amount of water adhere to the tread as the tire turns back for a time, forming the tail wave. The sketches of tire spray are shown in Fig.1.

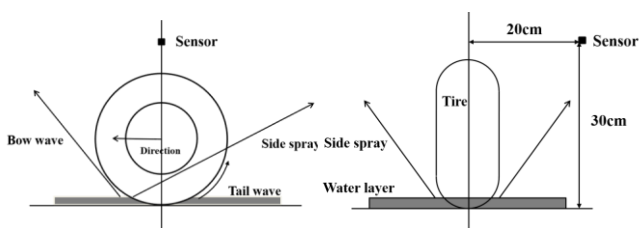

(a) side view of tire and side spray (b) front view of tire and side spray
Fig.1 The sketches of tire water spray

Tire drop experiment

The tire splash experiment in this paper is the tire drop experiment. Compared with the rolling tire splash experiment, the site of the tire drop experiment can be simpler. The experiment platform is relatively simple to build, and the experiment process can be greatly simplified. At the same time, it is also possible to better photograph the spray patterns and measure the impact load of water spray. Therefore, this study uses the tire drop experiment to verify the validity of impact load calculation.
The experiment platform is constructed as shown in Fig. 2.

Fig.2 Platform of the tire drop experiment

Table 1. Parameters of the tire drop experiment

Parameters of the tire	Diameter (outer)	Diameter (inner)	Pressure	width
	250mm	95mm	0.138Mpa	80mm
Experimental parameters	Water depth	Height		Sensor position
	20mm	30cm/50cm		(20cm,30cm)

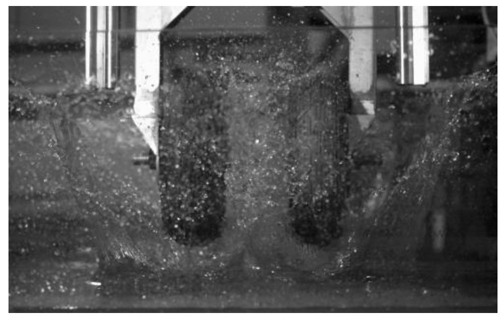

Fig.3 Tire spray pattern

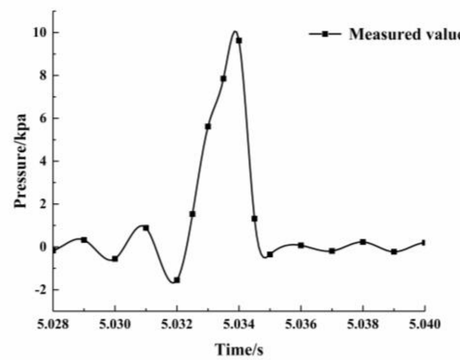

(a) 30mm height

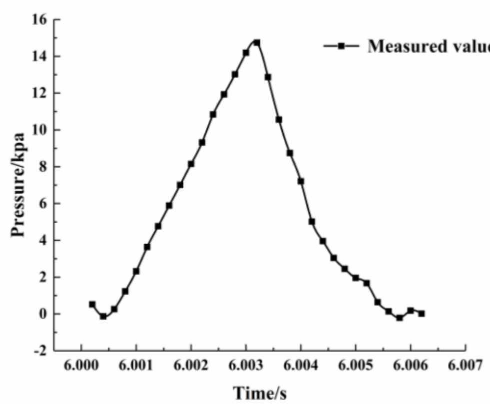

(b) 50mm height
Fig.4 Tire spray impact load

Before the tire drop experiment, the geometric parameters of the tire and the tire pressure are measured first. At the same time, the tire static load test is carried out to get the pressure-load relationship of the tire, and the deformation of the tire under the force of 800N is 10mm. The parameters of the experiment are shown in the table1. The sensor is 20cm from the outside of the bottom of the tire, and the height of the sensor is 30cm. The location of the sensor is marked in Fig.1. The tires are lifted to different heights and released, and then the experiment is repeated five times for each height. A high-speed camera is used to capture tire spray patterns.

A spray pattern captured by the high-speed camera is shown in Fig. 3. The spray impact load measured by the sensor is shown in Fig. 4. The impact load of different conditions can be obtained by using the Pauta (3 σ) criterion to exclude outliers. The processing of the measured data is shown in Table 2.

Table 2. Measured values of spray impact load

Height/30cm	Measured value/kpa	Error/kpa
1	10.58	0.8622
2	9.812	0.0942
3	10.212	0.4942
4	7.473(abandoned)	2.2448
5	10.512	0.7942
Average value	9.7178	If the error is larger than 3 σ , the data should be abandoned
Root mean square error (σ)	0.64(3 σ =1.92)	
Corrected average	10.279	
Height/30cm	Measured value/kpa	Error/kpa
1	16.659	3.032
2	9.7354	3.8916
3	14.549	0.922
4	14.737	1.11
5	12.458	1.169
Average value	13.627	If the error is larger than 3 σ , the data should be abandoned
Root mean square error (σ)	2.13(3 σ =6.39)	
Corrected average	13.627	

Tire Spray Model

Tire model

In this paper, the finite element model of a tire is established in Hypermesh based on the data of the experimental tire and imported into LS-DYNA. The actual configuration of a tire is very complex, composed of tread, belt layer, side wall, wire coil, inner tube, tire curtain layer and tire hub. The tire spray patterns are only related to the shape and deformation of the tire, so the tire model is simplified, only including the tread, side wall, inner tire and rim (a simplified version of the hub), as shown in Fig.5. The tread and sidewall are made of Mooney-Rivlin material. Mooney-Rivlin material is a kind of hyperelastic material, which is usually used to simulate rubber. The inner tire is made of elastic material, and the rim is made of rigid material. A uniformly distributed pressure of 0.138 MPa is applied to the normal direction of the inner tire tread to simulate the tire pressure of a pneumatic tire.

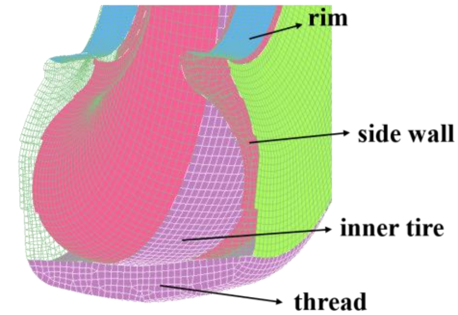

Fig.5 Tire configuration

The particle spacing of the water model was set to 2mm. The geometric parameters of the water film are as follows: 200 mm width (in the X direction), 200 mm length (in the Y direction length), and 20 mm depth (in the Z direction). The total number of particles is 1 million. The tire spray model is shown in Fig. 6.

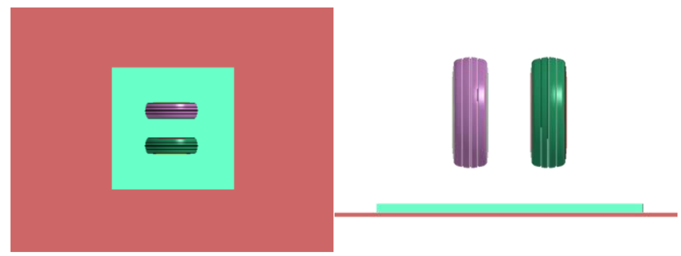

(a) plan view of tire spray model (b) front view of tire spray model

Fig.6 Tire water spray model

SPH method

The SPH method is an N-body integration scheme, which avoids the limitations of mesh tangling encountered in large deformation problems with the FEM. The main difference between SPH and traditional mesh methods is the absence of the grid. Therefore, the particles are the computational framework on which the governing equations are resolved (Liu M B, Liu G R, Lam K Y 2003). The SPH method has been applied in much commercial software and has shown promising prospects in aircraft tire spray (J.O. Hallquist 2007).

The particle approximation of a function is written as:

$$\prod{}^{h} f(\mathbf{x}_i) = \sum_{j=1}^{N} w_j f(\mathbf{x}_j) W\left(\mathbf{x}_i - \mathbf{x}_j, h\right) \quad (1)$$

Where W is the kernel function, subscripts i and j are particle codes, N is the number of particles in the influence domain of particle i, $w_j = \dfrac{m_j}{\rho_j}$ is the weight of the particle, $\mathbf{x}$ is the coordinate of particle, m is the mass of the particle, and ρ is the density.

The Kernel function W is defined using the function θ by the relation:

$$W\left(\mathbf{x}, h\right) = \frac{1}{h\left(\mathbf{x}\right)^{d}} \theta\left(\mathbf{x}\right) \quad (2)$$

where d is the number of space dimensions, and h is the smoothing length, which varies in time and space. The $W(\mathbf{x}, h)$ should be a centrally peaked function.

The most common smoothing kernel used by the SPH community is the cubic β -spline, which is defined by choosing θ as:

$$\theta(u) = C \times \begin{cases} 1 - \frac{3}{2}u^2 + \frac{3}{4}u^3 & |u| \le 1 \\ \frac{1}{4}(2-u)^3 & 1 \le |u| \le 2 \\ 0 & |u| > 2 \end{cases} \tag{3}$$

where C is a constant of normalization that depends on the number of dimensions.

The continuity equation, moment equation, and energy equation are:

$$\frac{d\rho}{dt} = -\rho \frac{\partial v^\beta}{\partial x^\beta} \tag{4}$$

$$\frac{d\mathbf{v}^\alpha}{dt}(\mathbf{x}_i(t)) = \frac{1}{\rho_i} \frac{\partial(\sigma^{\alpha\beta})}{\partial x_i}(\mathbf{x}_i(t)) \tag{5}$$

$$\frac{dE}{dt} = -\frac{p}{\rho} \nabla \cdot \mathbf{v} \tag{6}$$

The discrete forms of momentum conservation equation and energy conservation equation in the SPH method are:

$$\frac{d\rho_i}{dt} = \rho_i \sum_{j=1}^{N} \frac{m_j}{\rho_j}(v_i^\beta - v_j^\beta) \bullet \frac{\partial W_{ij}}{\partial x_i^\beta} \tag{7}$$

$$\frac{d\mathbf{v}^a(\mathbf{x}_i)}{dt} = \sum_{j=1}^{N} m_j \left(\frac{\sigma^{\alpha,\beta}(\mathbf{x}_i)}{\rho_i^2} A_{ij} - \frac{\sigma^{\alpha,\beta}(\mathbf{x}_i)}{\rho_j^2} A_{ji} \right) \tag{8}$$

$$\frac{dE(\mathbf{x}_i)}{dt} = -\frac{p_i}{\rho_i^2} \sum_{j=1}^{N} m_j \left(v(\mathbf{x}_j) - v(\mathbf{x}_i) \right) A_{ij} \tag{9}$$

$$\sigma^{\alpha\beta} = -p\delta^{\alpha\beta} + \tau^{\alpha\beta} \tag{10}$$

$$\tau^{\alpha\beta} = 2\mu\dot{\varepsilon}^{\alpha\beta} \tag{11}$$

where superscript α and β are the space indices, E is the internal energy, v is the velocity, σ is the total stress tensor, p is the isotropic pressure, t is the time, τ is the viscous stress, ε is the shear strain rate, μ is the viscosity coefficient, and $A_{ij} = \frac{1}{h^{d+1}}\theta'\left(\frac{\|x_i - x_j\|}{h}\right)$.

If we choose the smoothing function to be symmetric and add the artificial viscosity, equation 8 can lead to the following equation.

$$\frac{d\mathbf{v}^a(\mathbf{x}_i)}{dt} = \sum_{j=1}^{N} m_j \left(\frac{\sigma^{\alpha,\beta}(\mathbf{x}_i)}{\rho_i^2} + \frac{\sigma^{\alpha,\beta}(\mathbf{x}_j)}{\rho_j^2} + \prod_{ij} \right) A_{ij} \tag{12}$$

An artificial viscous pressure term $\prod_{ij}$ is added such that:

$$p_i \to p_i + \prod_{ij} \tag{13}$$

$$\prod_{ij} = \frac{1}{\bar{\rho}_{ij}}(-A\mu_{ij}\bar{c}_{ij} + D\mu_{ij}^2) \tag{14}$$

$$\mu_{ij} = \begin{cases} \bar{h}_{ij} \frac{v_{ij} r_{ij}}{r_{ij}^2 + \eta^2} & if \;\; v_{ij} r_{ij} < 0 \\ 0 & otherwise \end{cases} \tag{15}$$

where $v_{ij} = (v_i - v_j)$, $\eta^2 = 0.01\bar{h}_{ij}$, A is 0.06, D is 1.5, c is the adiabatic sound speed, and r_{ij} is the distance between particles i and j.

We use a classical and straightforward first-order scheme for integration. The time step is determined by the expression:

$$\delta t = C_{CFL} Min_i \left(\frac{h_i}{c_i + v_i}\right) \tag{16}$$

where the factor C_{CFL} is a numerical constant. It is usually 0.5.

The material property of water is simulated by combining a NULL material with a Gruneisen equation of state, which uses a cubic shock velocity and fluid particle velocity to determine the pressure of compressed and expanded water. The parameters are shown in Table 3. The Gruneisen equation of state with cubic shock velocity-particle velocity defines pressure for water as:

$$p = \frac{\rho_0 B^2 k \left[1 + \left(1 - \frac{\gamma_0}{2}\right)k - \frac{a}{2}k^2 \right]}{1 - (S_1 - 1)k - S_2 \frac{k^2}{k+1} - S_3 \frac{k^3}{(k+1)^2}} + (\gamma_0 + ak)E \tag{17}$$

where ρ_0 is the initial density, B is the intercept of the shock velocity-particle velocity curve, S_1, S_2 and S_3 are the coefficients of the slope of the shock velocity-particle velocity curve, γ_0 is the Gruneisen gamma, and a is the first order volume correction to γ_0. The compression k is defined in terms of the relative volume V as: $k = \frac{1}{V} - 1$.

Table 3. State equation parameters and material parameters of water

<table>
<tr><td rowspan="2">GRUNISEN function</td><td>C(m/s)</td><td>S₁</td><td>S₂</td><td>S₃</td><td>γ₀</td><td>a</td></tr>
<tr><td>1480</td><td>2.16</td><td>-1.985</td><td>0.2268</td><td>0.5</td><td>2.67</td></tr>
<tr><td rowspan="2" colspan="3">Null</td><td colspan="2">ρ₀(kg/m³)</td><td colspan="2">Mu(kg/(m s))</td></tr>
<tr><td colspan="2">1000</td><td colspan="2">0.00768</td></tr>
</table>

Calculation of spray impact load

Simulation of splashing trajectory

After the numerical simulation of the tire spray is completed, the calculation results are extracted. The spray patterns obtained from the simulation are in good agreement with the spray patterns captured by the camera. The position and velocity information of the water particles is exported.

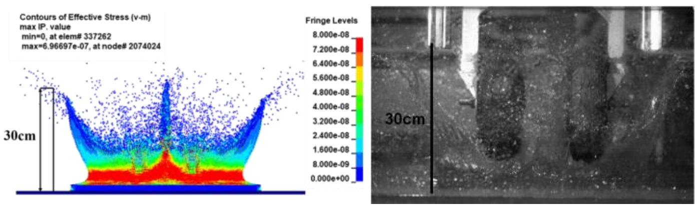

(a) 30cm height

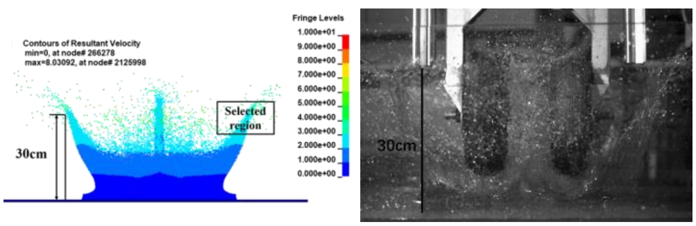

(b)50cm height

Fig 7 The patterns of tire water spray

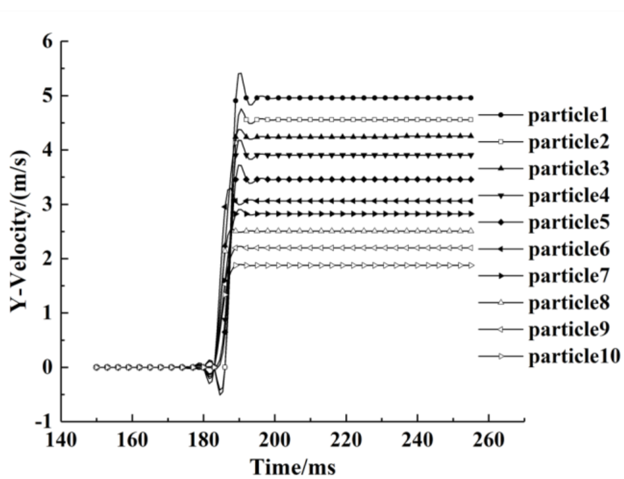

Fig. 8 Velocity curve of splashing particles

Fig. 8 is the velocity curve of the splashing particles belonging to the side spray, and the calculation of the particles in LS-DYNA is not affected by air. The selected region of the particles is shown in Fig. 7(b). The SPH particles can simulate the deformation, fragmentation, and fusion of liquid droplets, which connect each other by force determined by the kernel function. If the distance between particles is beyond the scope, the force between particles can be ignored. It can be seen from Fig. 8 that the velocity of the particles remains relatively stable after the particles form a side spray pattern. It shows that once the particles are dispersed, the force between the particles is negligible, and the motion of splashing particles will be affected by flow field and gravity.

The air resistance of the water particles in the engine flow field is:

$$F = \frac{1}{2}\rho v^2 A(l) C_d \tag{18}$$

$$F = \frac{1}{2}\rho v^2 A(l) C_d \tag{19}$$

The Reynolds number and the resistance coefficient are calculated as follows:

$$Re = \frac{\rho v d}{\mu} \tag{20}$$

$$C_d = \begin{cases} \dfrac{24}{Re}(1+0.15Re^{0.687}) & Re \le 1000 \\ 0.44 & Re > 1000 \end{cases} \tag{21}$$

The acceleration of the particle is calculated as follows:

$$\begin{cases} \dfrac{d^2x}{dt^2} = -\dfrac{3}{4}\dfrac{\rho_a}{\rho_w}\dfrac{C_d}{D}\mathbf{v}\cdot\mathbf{v}_x \\ \dfrac{d^2y}{dt^2} = -\dfrac{3}{4}\dfrac{\rho_a}{\rho_w}\dfrac{C_d}{D}\mathbf{v}\cdot\mathbf{v}_y \\ \dfrac{d^2z}{dt^2} = -\dfrac{3}{4}\dfrac{\rho_a}{\rho_w}\dfrac{C_d}{D}\mathbf{v}\cdot\mathbf{v}_z \end{cases} \tag{22}$$

where x, y and z are the particle coordinates, D is the diameter of the droplet, C_d is the air resistance coefficient, ρ_a is the air density, ρ_w is the water density, v is the droplet movement velocity, and $A(l)$ is the sectional droplet area. A program is written in MATLAB to calculate the subsequent trajectory of the tire spray under the influence of the flow field.

Calculation of impact load

After the complete trajectory of the tire spray is calculated, the position and velocity information of the splashing particles is saved. Then the spray pattern after *dt* time is calculated to get the velocity and position information of the splashing particles at the moment *t+dt*. The information of the splashing particles at both moments is imported into two matrices. The spatial position equation of the cross-section is determined according to the position of the sensor, and then the spatial position relationship is used to determine whether the particles cross the cross-section. The particles crossing the cross-section are regarded as droplets, and the impact load of each droplet is calculated and accumulated to obtain the impact load of the water spray.

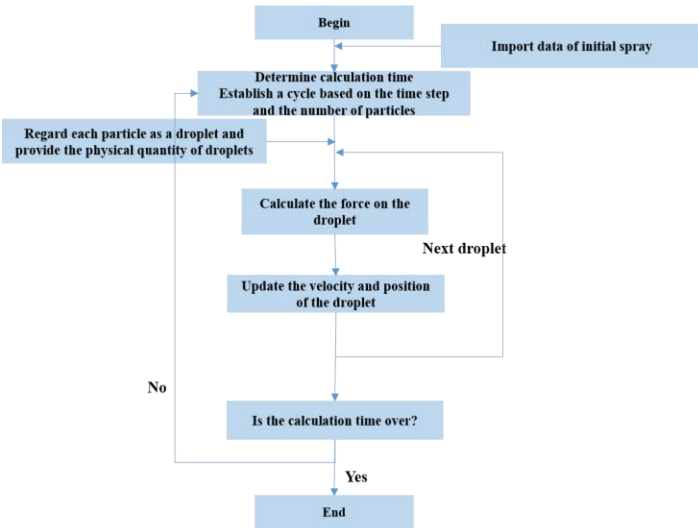

Fig. 9 Flow chart of droplet trajectory calculation

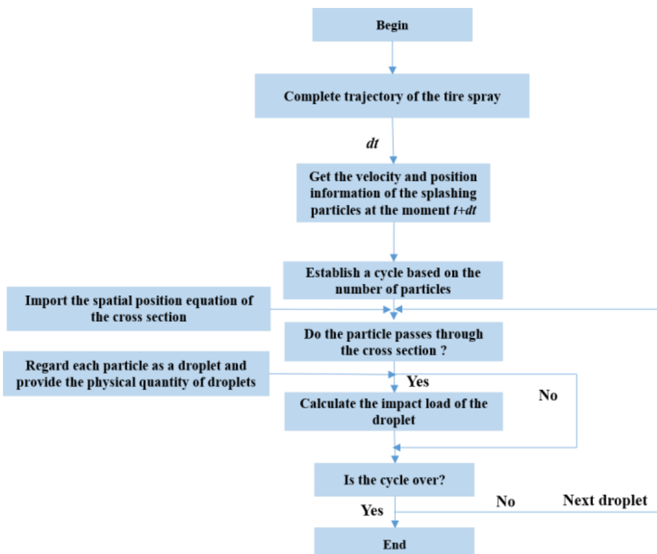

Fig. 10 Flow chart of impact load calculation

The calculation formulas for the impact load of a single droplet are as follows (Amrit Shankar Verma,Saullo G.P. Castro,Zhiyu Jiang,Julie J.E. Teuwen.2020)：

$$F = 0.84\rho_w V_{imp}{}^2 \phi_d{}^2 \tag{23}$$

$$I = 0.56 V_{imp}{}^{0.95} \phi_d{}^{2.98} \tag{24}$$

Where F is the maximum impact force of the droplet, I is the impulse during the impact of the droplet, ρ_w is the density of water, V_{imp} is the normal velocity of the droplet relative to the cross-section, and ϕ_d is the diameter of the droplet.

$$Re = \frac{\rho_w V_{imp} \phi_d}{\mu} > 230; \quad We = \frac{\rho_w V_{imp}{}^2 \phi_d}{\gamma} > 50 \tag{25}$$

where ρ_w, μ, γ are density, viscosity coefficient and surface tension respectively, which is for water taken as 1000 kg/m^3, 0.001 Pa.s and 73.42 mN/m in this study.

Eq. (23) and (24) are valid as long as the droplet is assumed spherical, and the droplet impact lies in the inertial dominated regime characterized by a Reynolds number (*Re*) greater than 230 and Weber number (*We*) greater than 50. According to Eq. (25), it is known that Eq. (23) and (24) are valid when the particle velocity exceeds 1.35m/s. According to Fig. 8, it can be seen that the velocity (Y direction) of all splashing particles exceeds 1.35m/s.

The calculation process of the spray impact load is shown in Fig. 10. The cross-section is in the plane where the sensor is located. The cross-sectional area of the sensor is very small, whose value is only 1 mm^2. If such a small area is chosen to calculate the impact load, the error is very large, so we choose a larger cross-sectional area centered on the sensor position. Similarly, if the time interval is set too small, the error will be large, and if it is set too large, the accuracy will be reduced. As a result, the effect of cross-sectional area and time interval on the spray impact load needs to be studied. The effect of cross-sectional area and time interval on the impact load is shown in Fig.11.

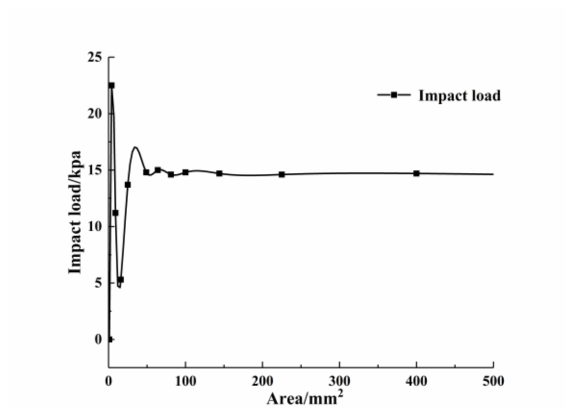

(a) area

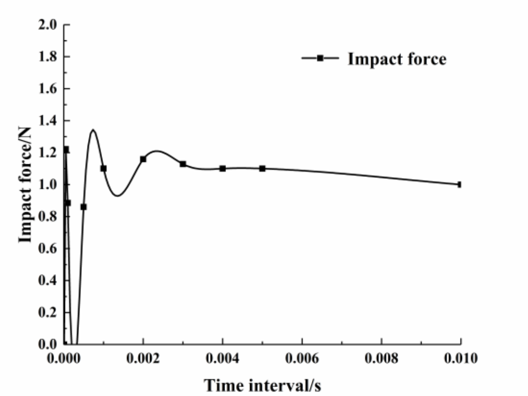

(b) time interval

Fig.11 Variation curve of impact load

When the cross-sectional area is less than 50mm^2, the value of impact load fluctuates greatly. When the cross-sectional area reaches 100 mm^2, the impact load starts to stabilize, so the actual cross-sectional area determined is a square area of 10 mm*10 mm. When the time interval is less than 1ms, the value of the impact force fluctuates greatly. The impact force reaches stability at 3ms and then starts to decrease slowly, so the actual time interval determined is 3ms.

The calculated results of impact load at different moments are shown in Table 4 and Fig.12.

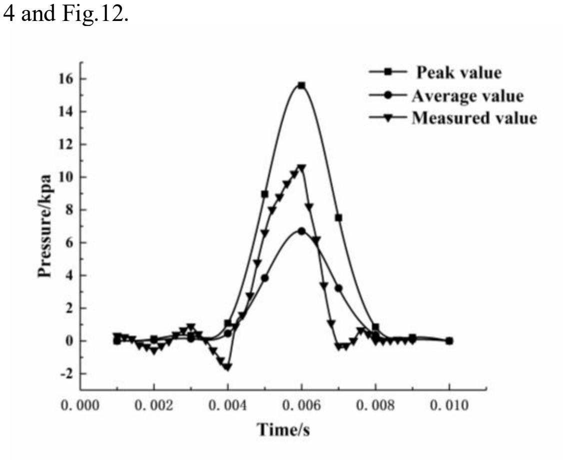

(a) 30mm height

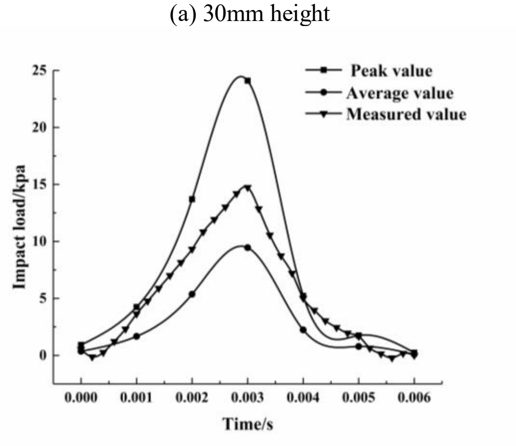

(b) 50mm height

Fig.12 Comparison of different values of impact load

Table 4. Different values of impact load

30cm height	Time/s	Peak value/kpa	Average value/kpa
1	0.001	0	0
2	0.002	0.05	0.05
3	0.003	0.14	0.14
4	0.004	1.08	0.46
5	0.005	8.96	3.84
6	0.006	15.59	6.7
7	0.007	7.52	3.22
8	0.008	0.85	0.36
50cm height	Time/s	Peak value/kpa	Average value/kpa
1	0.001	4.25	1.67
2	0.002	13.7	5.37
3	0.003	24.1	9.45
4	0.004	5.23	2.24
5	0.005	1.75	0.78

Table 4 shows the peak and average values of impact load at different moments. As can be seen from the table, when the height is 30cm, the spray impact load reaches its maximum value at 0.006s, with a peak value of 15.59kpa and an average value of 6.7kpa. When the height is 50cm, the spray impact load reaches its maximum value at 0.003s, with a peak value of 24.1kpa and an average value of 9.45kpa. The measured value is between the average and peak values.

Correction of impact load

The peak and average values of the impact load do not match the actual values. The peak value is obtained by calculating the maximum impact force for each droplet passing through the cross-section. In practice, not all droplets will reach the maximum impact force at the same moment, so the calculation according to the maximum impact force will result in a calculated value that is larger than the measured value. The average value is obtained by calculating the impulse of each droplet passing through the section, so the average value is closer to the average impact force of the water spray on the section during this time interval. According to the average value, the calculation will result in the calculated value being small compared with the measured value. Therefore, the calculation method of impact load needs to be improved.

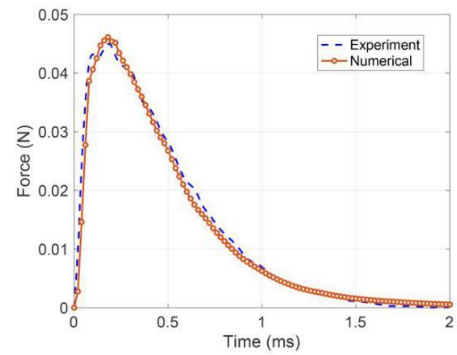

Fig.13 Variation curve of droplet impact force with time

Fig.13 (Amrit Shankar Verma,Saullo G.P. Castro,Zhiyu Jiang,Julie J.E. Teuwen) shows the relationship between a droplet impact force and time. In this paper, the researchers used the SPH method to simulate the impact process of a droplet on a blade, measured the impact load of the droplet, and compared it with the experimental results. The ϕ_d (diameter of the droplet in his paper) is 2.7mm, and the V_{imp} is 2.67m/s. According to Eq.23, the maximum impact force of the droplet is 0.0437N.

The curve is fitted by polynomial interpolation to obtain the equation of the impact force of a droplet on the plate with respect to time. The time of a droplet impacting the plane is 2ms.

$$y(t) = 0.3901t^9 - 3.66t^8 + 14.55t^7 - 31.91t^6 + 42.33t^5 \\ -34.73t^4 + 17.65t^3 - 5.326t^2 + 0.8038t - 0.001519 \tag{26}$$

After obtaining the fitted equation of droplet impact force versus time, the Monte Carlo method can be used to calculate the spray impact load. If there are n droplets crossing the cross-section, then the moment t occupied by the particle i $(i<=n)$ is located is $i*(2/n)$. The maximum impact force of the droplet is F_{max}. Then the impact force of this droplet is $(F_{max}/0.0437)*y(i*2/n)$. However, if the impact force of the droplets through the section is uniformly distributed according to the fitted equation, the expected value of the impact load is calculated, which is not essentially different from the average value. Therefore, the Monte Carlo method should be corrected.

When the peak value of impact load is measured in the experiment, it must be when the droplets hitting the pressure sensor are at the maximum impact force. The droplet distribution is not following with the uniform distribution, so the Monte Carlo algorithm needs to be corrected. The droplets are selected, whose cross-sectional area is equal to 100 mm^2, and the impact force of these droplets is set to the maximum impact force. The impact force of the other droplets is then uniformly distributed according to the fitted equation to obtain the corrected impact load of water spray. The results are shown in Fig.14 and Table 5.

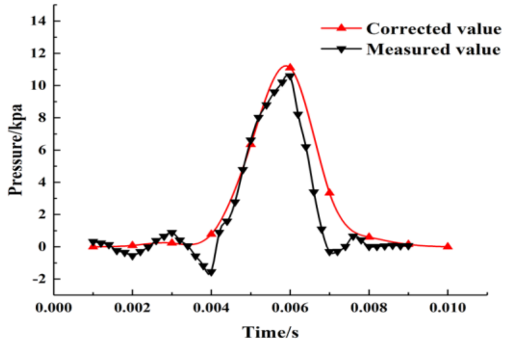

(a) 30mm height

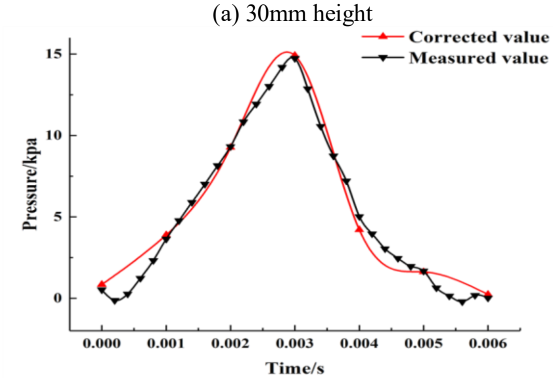

(b)50mm height

Fig.14 Comparison of corrected values with measured values

Table 5. Corrected values of impact load

	Peak value	Average value	Corrected value	Measured value
50cm	24.1kpa	9.45kpa	14.91kpa	13.627kpa
30cm	15.2848kpa	6.7kpa	11.19kpa	10.279kpa

The values of impact load obtained by the Monte Carlo correction algorithm are the closest to the measured values, with an error of 8.86% under 30cm height working condition and an error of 9.4% under 50cm height working condition. The curves of the corrected value and the measured value with time are also in good agreement.

CONCLUSIONS

In this paper, the SPH-FEM method is used to simulate the spray patterns after the vertical descent of the tire, and the spray patterns are in good agreement with the patterns captured by the camera.

The SPH particles are discrete into droplets, then the trajectory of splashing particles in the airflow field is simulated, and the impact load of spray water is calculated. The impact load of water spray on the sensor is calculated by the corrected Monte Carlo method, which is in good agreement with the measured value.

The calculation method proposed in this paper based on the SPH method can calculate the subsequent trajectory of water spray and impact load after obtaining the distribution of the initial spray. Compared with the numerical simulation of the whole process, the computational scale is reduced, and the computational efficiency is improved.

ACKNOWLEDGEMENTS

This work is supported by National Natural Science Foundation of China (52131102, 51879159), and the National Key Research and Development Program of China (2019YFB1704200), to which the authors are most grateful.

REFERENCES

Amrit SV, Saullo GP, Jiang, Z, Julie JE (2020). "Numerical investigation of rain droplet impact on offshore wind turbine blades under different rainfall conditions: A parametric study". *Composite Structures*, 241.

ESDU (1998). "Estimation of Spray Patterns Generated from the Sides of Aircraft Tyres Running in Water or Slush", *ESDU 83042*.

FAA. (2015). "Takeoff performance data for operations on contaminated runways", *AC 25-31*.

Gooden, JHM (2012). "The effect of crosswind on engine ingestion during take-offs from water contaminated runways". *28th International Congress of the Aeronautical Sciences*.

Gooden, JHM (2013). "Engine Ingestion as a Result of Crosswind During Take-Offs from Water Contaminated Runways", *NLR-TP-2013-201*.

Gotoh H, Khayyer A (2021). "Shimizu Y . Entirely Lagrangian meshfree computational methods for hydroelastic fluid-structure interactions in ocean engineering—Reliability, adaptivity and generality – ScienceDirect". Applied Ocean Research, 115:102822.

Guan X, Xu F, Hu M (2021). "Numerical Simulation of Water Spray Generated by Aircraft Multi-Wheels". *International Journal of Computational Fluid Dynamics*, 35(1-2).

Hallquist, JO (2007). "LS-DYNA Keyword User's Manual", *Livermore Software Technology Corporation*.

Khayyer A, Shimizu Y, Gotoh H (2021). "A coupled Incompressible SPH-Hamiltonian SPH solver for hydroelastic FSI corresponding to composite structures". Applied Mathematical Modelling, 94(1).

Liu MB, Liu GR, Lam KY (2003). "Smoothed particle hydrodynamics for numerical simulation of underwater explosion". *Computational Mechanics*, 30(2):106—118.

Liu MB, Zong Z, Chang JZ (2011). "Developments and applications of smoothed particle hydrodynamics". *Advances in Mechanics*, 41: 217-234.

Luo M, Khayyer A, Lin PZ (2021). "Particle methods in ocean and coastal engineering". Applied Ocean Research,114.

Van Es GWH, Roelen ALC, Kruijsen EAC (1998). "Safety aspects of aircraft performance on wet and contaminated runways". *10th Annual European Aviation Safety Seminar*. Amsterdam: National Aerospace Laboratory.

You Y, Khayyer A, Zheng X (2021). "Enhancement of δ-SPH for ocean engineering applications through incorporation of a background mesh scheme". Applied Ocean Research, 1: 102508.

Zhang X, Xu F, Ren X, Gao X, Cao R (2019). "Consideration on aircraft tire spray when running on wet runways". Chinese Journal of Aeronautics.

Zhao K, Liu PQ, Qu QL, (2017). "Numerical Simulation of Aircraft Tire-Generated Spray and Engine Ingestion on Flooded Runways". Journal of Aircraft, 1-9.

Zhao K, Liu PQ, Qu QL (2018). "Flow physics and chine control of the water spray generated by an aircraft rigid tire rolling on contaminated runways". Aerospace Science and Technology, 72:49-62